The effects of high content Tin (Sn) doping on the layered $LiMnO_2$ cathode material for lithium-ion batteries.

Bridget Mokgabudi[1*], *Kemeridge* Malatji[1], *Noko* Ngoepe[1] “and *Phuti* Ngoepe[1]

[1]Materials Modelling Centre, University of Limpopo, Private Bag x1106, Sovenga 0727, South Africa.”

Abstract. The search for advanced cathode materials is intensifying to meet the growing demand for high performance lithium-ion batteries from renewable energy and electric vehicle sectors. Lithium transition metal oxides ($LiMO_2$), especially $LiMnO_2$ are highly promising candidates due to their high capacity, energy density, thermal stability, and low cost. However, the practical use of $LiMnO_2$ is hindered by its structural instability and significant capacity fade, primarily caused by the Jahn-Teller distortion of Mn^{3+} ions. In this study, cluster expansion (CE) and density functional theory (DFT) were utilized to explore Sn-doped $LiMnO_2$ as a promising cathode material for lithium-ion batteries. A total of 29 Sn-doped configurations were generated, with three identified as lying on the binary ground state line. Among these, the phase $Li_4MnSn_3O_8$, corresponding to a 25:75 Mn-Sn ratio, was examined in detail. This phase crystallizes in a triclinic structure and exhibits thermodynamic stability, evidenced by its negative formation energy. Electronic structure calculations indicate semiconducting behaviour with a clear band gap and minimal contribution from Sn to the density of states. Additionally, mechanical analysis confirms the material's ductile nature, implying good deformation tolerance. Overall, these results offer valuable insights into the stability, electronic properties, and mechanical behaviour of Sn-doped $LiMnO_2$ for battery applications.

1 Introduction

Lithium-ion batteries (LIBs) dominate modern energy storage, powering electric vehicles, grid systems, and portable electronics due to their high energy density, long cycle life, and efficiency [1–3]. As renewable energy adoption grows, LIBs are critical for enabling large-scale storage and electrified transportation [4]. However, the performance and sustainability of these batteries depend heavily on cathode materials.

Conventional cathode materials like $LiMnO_2$ suffer from electrochemical instability, while lithium-rich layered oxides offer higher capacities through combined cationic and anionic redox activity [5]. Among these, Sn-based layered oxides are particularly promising

---

[*] Corresponding author: bridgetmokgabudi02@gmail.com

due to their high capacity and low cost, yet challenges in structural stability and cycling efficiency persist [6].

Doping strategies, such as substituting transition metals (Co, Ni, Sn) or incorporating anions (F, P), have been employed to enhance cathode performance [8, 9]. Cobalt's low natural abundance results in high cost. Furthermore, its toxicity and negative environmental impact present significant development challenges [10]. Tin doping improves $LiMnO_2$ stability by facilitating lithium-ion mobility and suppressing phase transitions, leading to better cycling performance [11], it is thermodynamically stable, soft and ductile [12]. Despite these advances, further optimization is needed to achieve commercially viable high-energy-density cathodes.

This study investigates the effect of Sn doping on $LiMnO_2$ cathode material, focusing on its impact on structural stability and electrochemical behaviour.

2 Methodology

The $LiMnO_2$ layered structure was initially doped with Sn at the 2a Wyckoff positions of Mn to maintain stoichiometric equivalence between Sn and Mn. The MedeA-Universal Cluster Expansion (UNCLE) [13] package was used to construct and automatically converge the Cluster Expansion (CE) for Sn-doped $LiMnO_2$, leading to the generation of new stable phases. Density functional theory (DFT) calculations were performed using the Vienna Ab Initio Simulation Package (VASP) [14] to evaluate the structural, electronic, and mechanical properties. The generalized gradient approximation with Perdew-Burke-Ernzerhof (GGA-PBE) [15] correlation functional was used. All the calculations were done using the cut-off energy of 500 eV and the Brillouin zone sampling scheme of Monkhorst-pack with 6x6x6 k-points mesh [16].

3 Results and discussion

3.1 Binary phase diagram

The cluster expansion simulations reveal critical insights into the thermodynamic stability of Sn-doped $LiMnO_2$, as illustrated in the binary ground state diagram (Figure 1). Three of the 29 generated phases lie on the DFT ground-state line (red line) in Fig. 1, indicating exceptional stability within the compositional space. These stable configurations emerge from a broader set of predicted phases (grey crosses) and training-set structures (green crosses and squares), which collectively map the system's energy landscape, including miscibility gaps and stable solid solutions. The cross-validation score (CVS) of <5 meV/position confirms the reliability of these predictions, underscoring the viability of Sn-doped phases for practical applications. Notably, the identification of stable phases at specific Sn/Mn ratios provides a foundation for targeting optimal compositions in experimental synthesis.

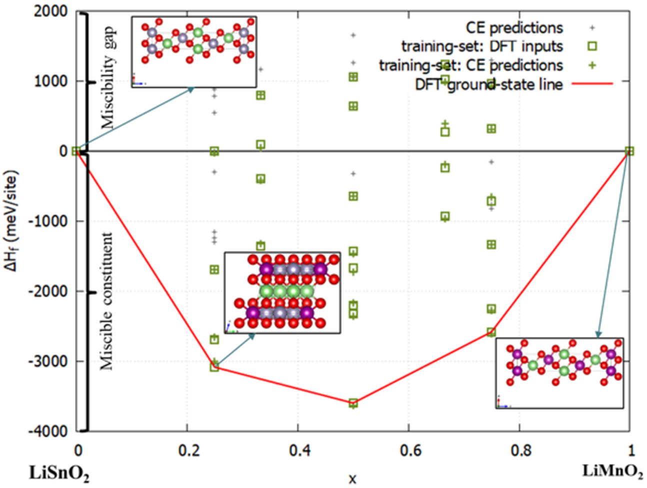

Fig. 1. Binary ground-state diagram of the Sn-doped $LiMnO_2$ system illustrating the generated phases and the most stable generated phases that lie on the DFT ground state line.

3.2 Structural properties

Full geometry optimization of atomic structures was performed with complete relaxation of atomic positions and unit cell parameters, yielding the crystallographic data in Table 1. The optimized $Li_4MnSn_3O_8$ phase adopts a triclinic P1 space group, evidenced by three unequal lattice constants (a = 6.029 Å, b = 6.083 Å, c = 6.148 Å) and non-orthogonal angles (α = 86.944°, β = 88.694°, γ = 117.993°). This minimal symmetry configuration, containing only translational periodicity, accommodates significant structural distortions arising from both Jahn-Teller effects of Mn^{3+} and strain from Sn incorporation. The resulting unit cell volume (198.52 Å^3) shows a 48.94% expansion versus undoped $LiMnO_2$ (~97 Å^3), consistent with the larger ionic radius of Sn^{4+} (0.69 Å) replacing Mn^{3+} (0.645 Å), which may enhance lithium-ion diffusion while reducing mechanical strain during cycling.

The phase exhibits exceptional thermodynamic stability, as demonstrated by its strongly negative heat of formation (-2494.58 kJ/mol) nearly 3.5 times greater than that of undoped $LiMnO_2$ (-700 kJ/mol). This remarkable stability, combined with its expanded yet distorted structure, suggests superior electrochemical performance for battery applications. The experimental lattice parameters (a = 2.805 Å, b = 2.809 Å, c = 4.572 Å) [17] and stabilization energy validate our cluster expansion predictions, confirming $Li_4MnSn_3O_8$ as a promising high-stability cathode material candidate in the Sn-doped $LiMnO_2$ system.

Table 1. Calculated lattice parameters, cell volume and energy of formation.

	Lattice parameters						**Volume (Å)**	**Heats of formation (kJ/mol)**
	a	b	c	α	β	γ		
$LiMnO_2$	2.833	2.833	5.097	90.000	90.000	120.000	97.164	-700.94
$Li_4MnSn_3O_8$	6.029	6.083	6.148	86.944	88.694	117.993	198.52	-2494.58

3.3 Density of states

To study the impact of Sn on the conductivity of the $Li_4MnSn_3O_8$ material, the Total and Partial Density of States (TDOS) and PDOS of the stable Sn phase was calculated and the results are displayed in figure 2 below.

The spin-polarized density of states (DOS) of $Li_4MnSn_3O_8$ reveals significant electronic modifications due to Sn doping. The spectrum is dominated by three key energy regions. First, at the valence band edge (−1.5 to 0 eV relative to the Fermi level), strong Mn-3d/O-2p hybridization occurs, with a peak at −0.8 eV, driving p-type conductivity. Next, the band gap region (0 to 0.566 eV) exhibits complete state depletion, confirming a defect-free semiconducting behaviour. In the conduction band (0.566–3 eV), unoccupied Mn-3d states, with a peak at 1.2 eV, provide efficient electron-accepting pathways. Interestingly, the Sn-5s/5p orbitals contribute minimally, with less than 5% partial density of states (PDOS) intensity across all regions, highlighting their role in structural stabilization rather than in electronic behaviour.

The comparative analysis with undoped $LiMnO_2$ reveals the dual effects of Sn doping. The band gap is significantly reduced from 0.797 eV in the pristine material to 0.566 eV in the doped system, which enhances the intrinsic carrier concentration. Additionally, the Fermi level shifts deeper into the valence band by +0.3 thereby strengthening the p-type character. However, the system ($Li_4MnSn_3O_8$) shows weaker Li-2p contributions in the conduction band indicating a slight reduction in Li^+ mobility. This trade-off is likely due to the structural stabilization provided by Sn doping [18].

These results demonstrate that while Sn doping optimizes electronic conductivity through gap engineering and enhanced Mn-O covalency, it requires careful balancing to maintain Li^+ transport, guiding future compositional tuning (e.g., Sn/Mn ratio optimization).

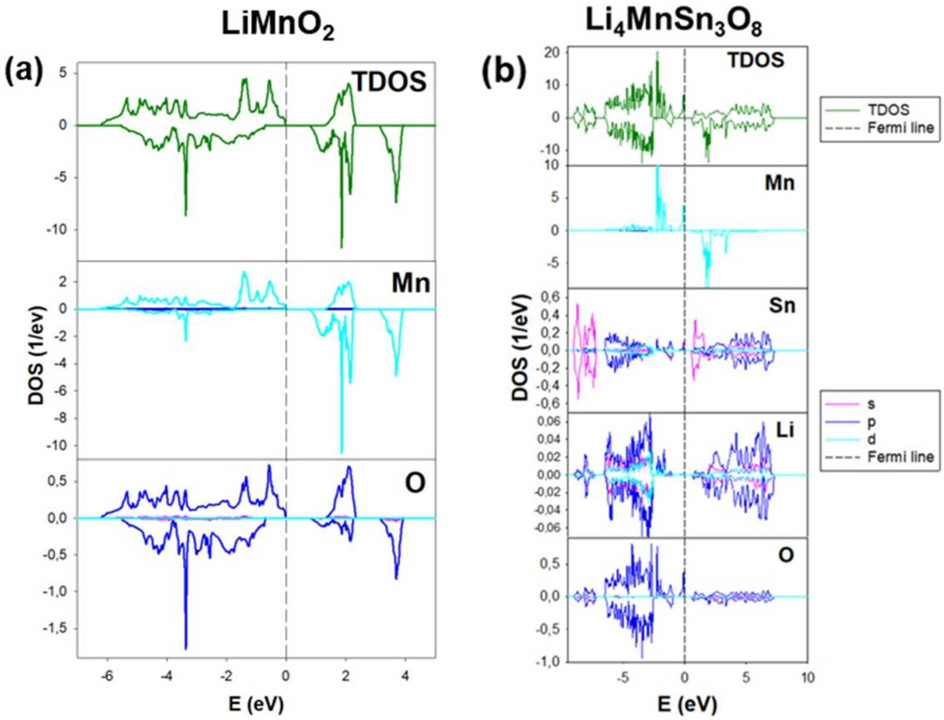

Fig. 2. The total density and partial density of states of(a) $LiMnO_2$ and (b) $Li_4MnSn_3O_8$.

3.4 Band structures

To clarify the electronic characteristics of $Li_4MnSn_3O_8$, we conducted first-principles calculations of its band structure along high-symmetry directions in the Brillouin zone. The analysis of these electronic bands provides fundamental insights into the conductive behaviour of the material. Our results demonstrate that $Li_4MnSn_3O_8$ exhibits semiconducting properties, as evidenced by the presence of an indirect band gap measuring 0.566 eV (Figure 3). In this indirect gap configuration, the valence band maximum and conduction band minimum occur at different crystal momentum points, a feature that significantly influences the electronic transport properties of the material. The magnitude of this band gap places $Li_4MnSn_3O_8$ in the category of narrow-gap semiconductors, suggesting potential for tuneable electronic applications where moderate charge carrier excitation is desirable. This electronic structure characterization forms a crucial foundation for understanding and potentially engineering the material's conductive properties for specific technological implementations.

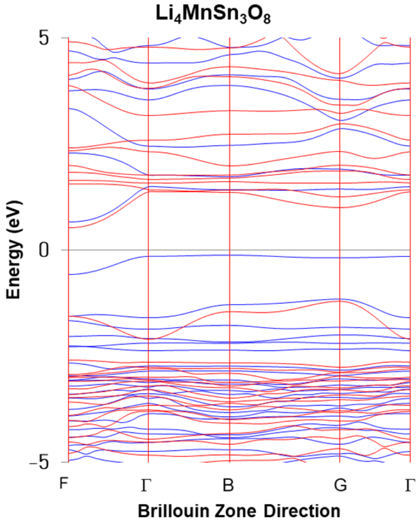

Fig. 3. Electronic band structure of $Li_4MnSn_3O_8$.

3.5 Mechanical properties

The strength and hardness of a material can be determined by analysing the elastic properties, as they reveal the response to phase transitions and interatomic stresses through elastic constants.

Elastic constants were calculated to evaluate the mechanical stability of the generated structure. These elastic constants were calculated under a strain of 0.005 and the results are shown in table 2 below to check the amount of strain in which the structures can withstand. Elastic properties are significant for determining the strength and hardness of the materials since elastic constants indicates how well the material responds to interatomic forces and phase transitions [19]. For the materials to be considered mechanically stable their lattice constants must adhere to the mechanical stability criteria of their crystal shapes. $Li_4MnSn_3O_8$ is a triclinic crystal and needs to adhere to the relevant mechanical stability criteria for such crystals [18] listed in expressions 3.2.1-3.54 below to be considered mechanically stable.

$C_{11}>0, C_{22}>0, C_{33}>0, C_{44}>0, C_{55}>0, C_{66}>0$

$$[c_{11}+c_{22}+c_{33}+2\times(c_{12}+c_{13}+c_{23})]>0 \tag{3.5.1}$$

$$(c_{33}\times c_{55}-c_{35}^2)>0 \tag{3.5.2}$$

$$(c_{44}\times c_{66}-c_{46}^2)>0 \tag{3.5.3}$$

$$(c_{22}+c_{33}-2\times c_{23})>0 \tag{3.5.4}$$

The triclinic crystal symmetry has 21 independent elastic constants C_{ij} (C_{11}, C_{12}, C_{13}, C_{14}, C_{15}, C_{16}, C_{22}, C_{23}, C_{24}, C_{25}, C_{26}, C_{33}, C_{34}, C_{35}, C_{36}, C_{44}, C_{45}, C_{46}, C_{55}, C_{56} and C_{66}. The constants need to satisfy $C_{11}>0$, $C_{22}>0$, $C_{33}>0$, $C_{44}>0$, $C_{55}>0$, $C_{66}>0$ [19]. The elastic constants of $Li_4MnSn_3O_8$ satisfy the mechanical stability criteria and all diagonal elements are positive (C_{11}, C_{22}, C_{33}, C_{44}, C_{55}, C_{66}) hence confirming its mechanical stability [20].

Table 2. Elastic constants for $Li_4MnSn_3O_8$.

Elastic constants (GPa)	**$Li_4MnSn_3O_8$**
C_{11}	117.39
C_{12}	54.67
C_{13}	42.37
C_{14}	-5.65
C_{15}	-0.14
C_{16}	12.87
C_{22}	184.60
C_{23}	67.72
C_{24}	-11.14
C_{25}	10.41
C_{26}	-15.42
C_{33}	166.35
C_{34}	-11.52
C_{35}	11.04
C_{36}	-7.69
C_{44}	63.25
C_{45}	-10.40
C_{46}	8.61
C_{55}	27.82
C_{56}	-5.92
C_{66}	64.20

To further study the mechanical stability of the Sn-doped structure, elastic moduli were calculated under a strain of 0.005 and the results are shown in table 3 below. $Li_4Mn_3SnO_8$ has positive values of the Bulk, Shear, and Young's modulus indicating that it has compressive strength, it is rigid and has resistance to elastic deformation. Ductility was assessed using Pugh's criterion, which suggest that a material is ductile if its ratio of bulk to shear modulus (B/G) exceeds 1.75; otherwise, it is considered brittle [21].

Table 3. Elastic constants for $Li_4MnSn_3O_8$.

Structure	Bulk (GPa)	Shear (GPa)	Young's (GPa)	Pugh's ratio	
$Li_4MnSn_3O_8$	85.13	46.97	118.98	1.812	Ductile

4 Conclusion

In this study, the structural, mechanical, and electronic properties of $Li_4MnSn_3O_8$ were systematically investigated using density functional theory (DFT) calculations. The compound crystallizes in a triclinic symmetry, and its stability was assessed through the binary ground state diagram and formation energy analysis. The high Sn content significantly enhances the structure thermodynamically stability, as evidenced by its negative formation energy and its position within the miscible constituent region of the phase diagram. While inducing a semiconducting electronic character with a well-defined band gap separating the valence and conduction bands. Notably, despite its high concentration, the contribution of Sn states to the overall DOS was found to be minimal. Furthermore, mechanical stability assessments confirm that the structure is ductile, suggesting favourable deformation characteristics. These comprehensive DFT-based insights provide a deeper understanding of the material's stability, electronic properties, and mechanical behaviour, which are crucial for potential applications in energy storage and electronic devices.

We sincerely acknowledge the National Research Foundation (NRF) for their financial support. This study utilized computational resources to run the calculations based within the Materials Modelling Centre (MMC) unit at the University of Limpopo and the Centre for High Performance Computing (CHPC) in Cape Town, South Africa.

The data reported in this paper is available upon request to the corresponding author.

References

1. R. N. Ramesha, C. P. Laisa, K. Ramesha, Improving electrochemical stability by transition metal cation doping for manganese in lithium-rich layered cathode, $Li_{1.2}Ni_{0.13}Co_{0.13}Mn_{0.54-x}M_xO_2$ (M= Co, Cr and Fe). Electrochim. Acta, **249**, 377–386 (2017). https://doi.org/10.1016/j.electacta.2017.08.039
2. B. Jeevanantham, M. K. Shobana, Enhanced cathode materials for advanced lithium-ion batteries using nickel-rich and lithium/manganese-rich LiNixMnyCozO2. J. Energy Storage, **54**, 105353 (2022). https://doi.org/10.1016/j.est.2022.105353
3. F. Wu, J. Maier, Y. Yu, Guidelines and trends for next-generation rechargeable lithium and lithium-ion batteries. chem. Soc. Rev. **49**,1569–1614 (2020). https://doi.org/10.1039/C7CS00863E
4. A.G. Olabi, Q. Abbas, P.A. Shinde, M.A. Abdelkareem, Rechargeable batteries: Technological advancement, challenges, current and emerging applications. Energy, **266**, 126408 (2023). https://doi.org/10.1016/j.energy.2022.126408
5. D. Huang, C. Engtrakul, S. Nanayakkara, D. Mulder, S. Han, M. Zhou, H. Luo, R. Tenent, Understanding degradation at the lithium-ion battery cathode/electrolyte interface: connecting transition-metal dissolution mechanisms to electrolyte composition. ACS Appl. Mater. Interfaces, **13**, 11930-11939 (2021). https://doi.org/10.1021/acsami.0c22235

6. F. R. Beck, R. Epur, D. Hong, A. Manivannan, P. N. Kumta, Microwave derived facile approach to Sn/graphene composite anodes for Lithium-ion batteries. Electrochim. Acta, **127**,299-306 (2014).

   https://doi:10.1016/j.electacta.2014.02.005
7. Z. Zhao, B. Zhang, L. Cheng, Z. Liu, J. Zou, J. Zhang, B. Huang, Enabling ultra-fast charging for Ni-rich $LiNi_{0.88}Co_{0.09}Mn_{0.03}O_2$ cathode by bulk W-doping. Mater. Lett, **306**,131043 (2022).

   https://doi:10.1016/j.matlet.2021.131043
8. X. Zhu, F. Meng, Q. Zhang, L. Xue, H. Zhu, S. Lan, Q. Liu, J. Zhao, Y. Zhuang, Q. Guo, B. Liu, L. Gu, X. Lu,Y. Ren, H. Xia, $LiMnO_2$ cathode stabilized by interfacial orbital ordering for sustainable lithium-ion batteries. Nat. Sustain, **4**, 392-401 (2021). https://doi.org/10.1038/s41893-020-00660-9
9. D. Linden, T.B. Reddy, *Handbook of Batteries*. 3rd edition, McGraw-Hill, (2002).
10. J. Ma, T. Liu, J. Ma, C. Zhang, J. Yang, Adv. Sci. **11**, 1–20 (2024). https://doi.org/10.1002/advs.202304938
11. H. Mou, W. Xiao, C. Miao, R. Li, L. Yu, Tin and Tin compound materials as anodes in Lithium-ion and Sodium-ion batteries: A review. Front. Chem, **8**, 1-14 (2020). https://doi.org/10.7209/carbon.020402
12. P.J. Smith, Ed., *Chemistry of Tin*. 2nd edition., (2012).
13. D. Lerch, O. Wiekhorst, G. L. W. Hart, R. W. Forcade, S. Muller, UNCLE: a code for constructing cluster expansions for arbitrary lattices with minimal user-input. Modell. Simul. Mater. Sci. Eng. **17**, 055003 (2009). https://doi.10.1088/0965-0393/17/5/055003
14. W. Yi, G. Tang, X. Chen, B. Yang, X. Liu, qvasp: A flexible toolkit for VASP users in materials simulations. Comput. Phys. Commun. **257**,107525 (2020). https://oi.10.1016/j.cpc.2020.107535
15. J. P. Perdew and W. Yue, Accurate and simple density functional for the electronic exchange energy: Generalized gradient approximation. Phys. Rev. B. **33**, 8800–8802, (1986). https://doi.10.1103/PhysRevB.33.8800
16. H.J. Monkhorst, J.D. Pack, Special points for Brillouin-zone integrations. Phys. Rev. B. **13**, 5188-5192 (1976). https://doi.org/10.1103/PhysRevB.13.5188
17. N.N. Shukla, R. Prasad, Electronic structure of $LiMnO_2$: A comparative study of the LSDA and LSDA+ U methods. J. Phys. Chem. Sol. **67**, 1731-1740 (2006). https://doi.org/10.1016/j.jpcs.2006.03.013
18. M. Morukuladi, N. Lethole, C. Masedi, P. Ngoepe, Investigating Stability Properties for Transition Metal Carbonate Precursors Using Universal Cluster Expansion Technique (UNCLE) as Cathodes for Li-Ion Batteries. J. Mater. Sci. Eng. A. **14**, 26–33 (2024). https://doi.10.17265/2161-6213/2023.1-3.004
19. Q. Guo, K. C. Lau, and R. Pandey, Thermodynamic and mechanical stability of crystalline phases of Li_2S_2. J. Phys. Chem. C. **123**, 4674-4681 (2019). https://doi.org/10.1021/acs.jpcc.8b11290
20. F. Mouhat and F. X. Coudert, Necessary and sufficient elastic stability conditions in various crystal systems. Phys. Rev. B. **90**, 224104 (2014). https://doi.10.1103/PhysRevB.90.224104
21. M. M. Hossain, First-principles study on the structural, elastic, electronic and optical properties of $LiNbO_3$. Heliyon, **5**, e01436 (2019). https://doi.10.1016/j.heliyon.2019.e01436